NJC

Cite this: *New J. Chem.*, 2012, **36**, 685–693

www.rsc.org/njc

PAPER

Piezofluorochromism and morphology of a new aggregation-induced emission compound derived from tetraphenylethylene and carbazole†

Xie Zhou,*[a] Haiyin Li,[b] Zhenguo Chi,*[b] Xiqi Zhang,[b] Jianyong Zhang,[b] Bingjia Xu,[b] Yi Zhang,[b] Siwei Liu[b] and Jiarui Xu*[b]

Received (in Montpellier, France) 8th September 2011, Accepted 19th November 2011
DOI: 10.1039/c1nj20782b

A new piezofluorochromic aggregation-induced emission compound was synthesized. The compound had morphology-alterable emission property and its amorphous and crystalline aggregates with various emissions were obtained through evaporation from the solutions in different solvent systems. The spectroscopic properties and morphological structures of the compound were reversed upon pressing and annealing (or fuming). The results show that the piezofluorochromic nature is generated through crystalline–amorphous phase transformation under external pressure. The reason for the phase transformation is ascribed to the twisted conformation of the molecule which leads to poor solid molecular packing and formation of some cavities in the interfaces of lamellar layers, as confirmed by single crystal X-ray diffraction analysis.

Introduction

Piezofluorochromic or piezochromic fluorescent material is a "smart" material whose fluorescent properties are changed in response to external pressure stimuli. Thus, piezofluorochromic material is also one class of typical mechano-responsive materials. The piezofluorochromic behavior can be achieved by changing the molecular chemical structures or the modes of solid state molecular packing. It is believed that the latter is easier than the former to realize dynamic controlling of solid state fluorescence with high efficiency and reversibility because the former is implemented using chemical reactions. It is well known that chemical reactions in the solid state frequently encounter insufficient conversion, irreversible reactions or loss of fluorescence ability of the previous compound. However, piezofluorochromic materials depended on the change of physical molecular packing modes are remaining extremely rare.[1] Recently, a series of wholly aromatic aggregation-induced emission compounds containing phenylvinylanthracene has been synthesized in our laboratory, and it is very interesting to find that some of them have piezofluorochromic nature.[2] We would thus suggest to call these compounds piezofluorochromic aggregation-induced emission (PAIE) materials as they possess both piezochromic fluorescence and aggregation-induced emission properties. Aggregation-induced emission materials are one of the important class of luminescent materials first reported by Tang's group.[3] They exhibit stronger emission in solid state than in solution, which offers a new path in solving the aggregation-caused quenching problem. They have attracted considerable research attention for many special properties such as strong emission in solid state, excellent device performance and highly stimuli-sensitive fluorescence.[4] To date, several types of aggregation-induced emission materials have been synthesized, including triphenylethylene, tetraphenylethylene, silole and cyano distyrylbenzene, and distyrylanthracene derivatives.[5] Recently, some PAIE compounds (**1–3**) were also reported by the other research groups[6] (Scheme 1), containing flexible and cyano groups in their molecular structures, which may result in low thermal stabilities such as low glass transition temperature and low decomposition temperature. Two-color luminescence switching behaviors of the compounds were explained by the interchange between metastable green-emitting G-phase and thermodynamically stable blue-emitting B-phase with different modes of local dipole coupling (antiparallel and head-to-tail arrangements, respectively), the origin for the interchange being the two-directional shear-sliding capability of molecular sheets formed *via* intermolecular multiple C–H···N and C–H···F hydrogen bonds. However, there are no such hydrogen bonds in the structures of our previously reported PAIE compounds. Thus, we proposed a mechanism, destruction of crystalline structure leads to the planarization of molecular conformation resulting in a red shift of photoluminescence (PL) spectrum, to explain the PAIE phenomenon.

[a] *School of Pharmaceutical Sciences, Sun Yat-sen University, Guangzhou 510275, China. E-mail: zhouxie@mail.sysu.edu.cn*
[b] *PCFM Lab, DSAPM Lab and KLGHEI of Environment and Energy Chemistry, FCM Institute, State Key Laboratory of Optoelectronic Materials and Technologies, School of Chemistry and Chemical Engineering, Sun Yat-sen University, Guangzhou 510275, China. E-mail: chizhg@mail.sysu.edu.cn, xjr@mail.sysu.edu.cn; Fax: +86 20 84112222; Tel: +86 20 84111081*

† Electronic supplementary information (ESI) available: Fig. S1–S10. CCDC reference number 815068. For ESI and crystallographic data in CIF or other electronic format see DOI: 10.1039/c1nj20782b

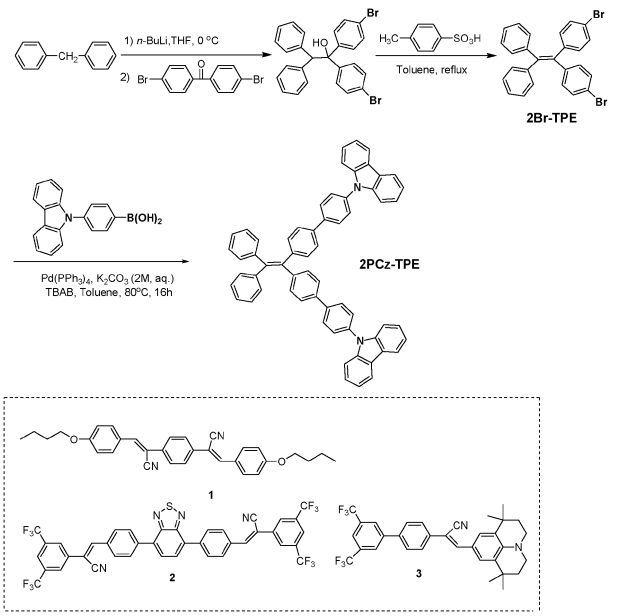

Scheme 1 Synthetic route for **2PCz-TPE** and the structures of the reported PAIE compounds (**1–3**).

Tetraphenylethylene-based derivatives possessed morphology-alterable emission property and some of them exhibited piezofluorochromic property,[7] which suggested that the tetraphenylethylene moiety should play a key role in determining the above properties.

In this article, we report a new "butterfly-shaped" piezofluorochromic aggregation-induced emission compound (**2PCz-TPE**) derived from tetraphenylethylene and carbazole with solid morphology-alterable emission. The single crystal of this compound has been successfully grown from the solution of dichloromethane/*n*-hexane mixture, which enabled us to determine its crystalline structure. The single crystal X-ray diffraction analysis reveals that the conformation of the **2PCz-TPE** molecule remains twisted in its crystalline state and there exist some cavities in the interfaces of lamellar layers due to the poor molecular packing. It is believed that this crystalline structure is readily destroyed by external pressure and this is the reason for why the compound exhibits PAIE property.

Experimental

Materials and measurements

Diphenylmethane, 4,4′-dibromobenzophenone, *n*-butyllithium in hexane (2.2 M), tetrakis(triphenylphosphine) palladium(0), tetrabutyl ammonium bromide (TBAB), and *p*-toluenesulfonic acid purchased from Alfa Aesar were used as received. 4-(9*H*-carbazol-9-yl)phenylboronic acid was obtained from Zhenjiang Haitong Chemical Industry Co., Ltd. (China). All other reagents and solvents were purchased as analytical grade from Guangzhou Dongzheng Company (China) and used without further purification. Proton and carbon nuclear magnetic resonance (^{1}H-NMR and ^{13}C-NMR) spectra were measured on a Mercury-Plus 300 spectrometer [$CDCl_3$, tetramethylsilane (TMS) as the internal standard]. Mass spectra (MS) were measured on a Thermo DSQ MS spectrometer. Elemental analyses (EA) were performed with an Elementar Vario EL elemental analyzer. The single crystal of the compound was grown from the dichloromethane/*n*-hexane mixture through slow volatilization. X-Ray crystallographic intensity data were collected at 110 K using a Bruker Smart 1000 CCD diffractometer equipped with a graphite monochromated enhance (Mo) X-ray source (λ = 0.71073 Å). The structure was solved by the direct methods following difference Fourier syntheses, and refined by the full-matrix least-squares method against F_0^2 using SHELXTL software (CCDC 815068).[8] Photoluminescence spectra (PL) were measured on a Shimadzu RF-5301pc spectrometer with a slit width of 1.5 nm for both excitation and emission. UV-vis absorption spectra (UV) were recorded on a Hitachi UV-vis spectrophotometer (U-3900). Differential scanning calorimetry (DSC) curves were obtained with a NETZSCH thermal analyzer (DSC 204 F1) at a heating rate of 10 °C min^{-1} under a N_2 atmosphere. Pressed samples were prepared by pressing the crystalline samples obtained from dichloromethane/*n*-hexane solution (1 : 3, v/v) in an IR pellet press at 1500 psi for 1 min. Annealing experiments were done on a hot-stage with an automatic temperature control system. The water/DMF mixtures with different water fractions were prepared by slowly adding distilled water into the DMF solution of samples under ultrasound at room temperature.

Synthesis of 2Br-TPE

A 2.2 M solution of *n*-butyllithium in hexane (9.1 mL, 20.0 mmol) was added to a solution of diphenylmethane (3.36 g, 20.0 mmol) in anhydrous tetrahydrofuran (50 mL) at 0 °C under an argon atmosphere. After stirring for 1 h at that temperature, the bis(4-bromophenyl)methanone (5.44 g, 16.0 mmol) was added and the reaction mixture was stirred for 10 h allowing the temperature to rise gradually to room temperature. Then the reaction was quenched with an aqueous solution of ammonium chloride and the mixture was extracted with dichloromethane. The organic layer was evaporated after drying with anhydrous sodium sulfate and the resulting crude hydroxy intermediate was dissolved in toluene (80 mL). The *p*-toluenesulfonic acid (0.68 g, 3.6 mmol) was added, and the mixture was refluxed for 12 h and cooled to room temperature. The mixture was evaporated and the crude product was purified by silica gel column chromatography using *n*-hexane as eluent to yield a light yellow powder (5.70 g, 73%). ^{1}H NMR (300 MHz, $CDCl_3$) δ (ppm): 6.82–6.90 (m, 4H), 6.95–7.05 (s, 4H), 7.06–7.16 (s, 6H), 7.18–7.27 (m, 4H); ^{13}C NMR (75 MHz, $CDCl_3$) δ (ppm): 120.93, 127.10, 128.10, 131.30, 133.20, 138.55, 142.38, 143.40; FT-IR (KBr) ν (cm^{-1}): 3053, 3021, 2354, 1590, 1480, 1434, 1382, 1065, 1007, 826, 761, 696, 482; MS (EI), *m*/*z*: 490 ([M]$^+$, calcd for $C_{26}H_{18}Br_2$, 490); Anal. calcd for $C_{26}H_{18}Br_2$: C, 63.70; H, 3.70; found: C, 63.65; H, 3.72.

Synthesis of 2PCz-TPE

To **2Br-TPE** (0.245 g, 0.5 mmol) and 4-(9*H*-carbazol-9-yl)-phenyl boronic acid (0.287 g, 1.0 mmol) in toluene (15 mL), 2 M aqueous K_2CO_3 solution (1.5 mL) and 0.010 g of TBAB were added. The mixture was stirred for 40 min under an argon atmosphere at room temperature. Then the $Pd(PPh_3)_4$

catalyst (catalytic amount) was added and the reaction mixture was stirred at 80 °C for 16 h. After cooling to room temperature, the product was concentrated and purified by silica gel column chromatography with CH_2Cl_2 : *n*-hexane (v : v, 1 : 3) to afford white powder (0.269 g, yield 66%). ^{1}H NMR (300 MHz, $CDCl_3$) δ (ppm): 7.10–7.20 (m, 10H), 7.21–7.25 (4H), 7.27–7.34 (m, 4H), 7.38–7.53 (m, 12H), 7.57–7.65 (d, 4H), 7.77–7.85 (d, 4H), 8.13–8.18 (d, 4H). ^{13}C NMR (75 MHz, $CDCl_3$) δ (ppm): 110, 120.15, 120.55, 123.70, 126.15, 126.50, 126.85, 127.50, 128.00, 128.40, 131.55, 132.25, 137.00, 138.23, 139.90, 140.08, 141.08, 141.96, 143.33, 143.85. FT-IR (KBr) ν (cm^{-1}): 3053, 2924, 2853, 1596, 1493, 1447, 1356, 1227, 1169, 1000, 819, 748, 722, 696, 618. MS (EI), *m*/*z*: 814 ($[M]^+$, calcd for $C_{62}H_{42}N_2$, 814). Anal. calcd for $C_{62}H_{42}N_2$: C, 91.37; H, 5.19; N, 3.44; found: C, 91.31; H, 5.16; N, 3.46.

Results and discussion

The synthetic route for the desired compound 9,9′-(4′,4″-(2,2-diphenylethene-1,1-diyl)bis(biphenyl-4′,4-diyl))bis(9*H*-carbazole) (**2PCz-TPE**) is illustrated in Scheme 1. The Suzuki coupling reaction of 4,4′-(2,2-diphenylethene-1,1-diyl)bis(bromobenzene) (**2Br-TPE**) with 4-(9*H*-carbazol-9-yl) phenylboronic acid provided the target compound with 66% yield. The molecular structures of the target compound and intermediates were confirmed by nuclear magnetic resonance (^{1}H-NMR, ^{13}C-NMR), Fourier transform infrared spectroscopy, elementary analysis, and mass spectrometry.

To confirm whether a compound is AIE-active or not, the fluorescent behaviors are usually studied by adding a poor solvent to the solution of the compound in a good solvent. As water is poor solvent and *N*,*N*-dimethylformamide (DMF) is good solvent for **2PCz-TPE**, the increase of the water fraction in the mixed solvent can change its existing form from a solution in pure DMF to aggregated particles in mixtures with high water content. The PL spectra of 10 μM of **2PCz-TPE** in the water/DMF mixtures with different water contents are shown in Fig. 1. The figure shows that if the water fraction is less than 20%, the PL intensity is very weak. However, a dramatic enhancement of emission is observed in the water/DMF mixture with water fraction >20%. The 1.1 PL intensity (a.u.) in pure DMF is elevated to 171.7 in the water/DMF mixture with water fraction of 40%, which is about 156-fold higher than that in the pure DMF solvent. This result indicates that the compound has strong AIE activity. The emission images of **2PCz-TPE** in pure DMF, 30% and 90% water fraction mixtures under 365 nm ultraviolet (UV) illumination are shown in Fig. 1 (inset). In pure DMF, the emission of the compound is very weak and virtually invisible. However, in 30% and 90% water fractions of water/DMF mixtures, the compound exhibits strong blue and green emissions, respectively. Upon comparing the images, PL spectra and UV spectra (Fig. 2) of the compound in the mixture with 30% and 90% water fractions are different. The difference is believed to indicate that the compound molecules pack in different modes in particles. According to their emission colors and PL spectra, molecules of **2PCz-TPE** form crystal-like aggregates (WAXD pattern is shown in Fig. S1, ESI†) and amorphous aggregates in mixtures with 30% and 90% water

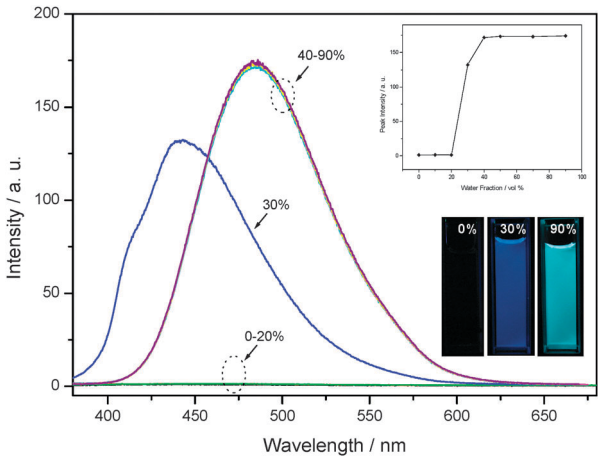

Fig. 1 PL spectra of the dilute solutions of **2PCz-TPE** in water/DMF mixtures with different volume fractions of water (concentration: 10 μM; excitation wavelength: 365 nm). [The inset shows the changes in PL peak intensity (up) and the emission images of **2PCz-TPE** in pure DMF, 30%, and 90% water fraction mixtures under 365 nm UV illumination (10 μM) (down)].

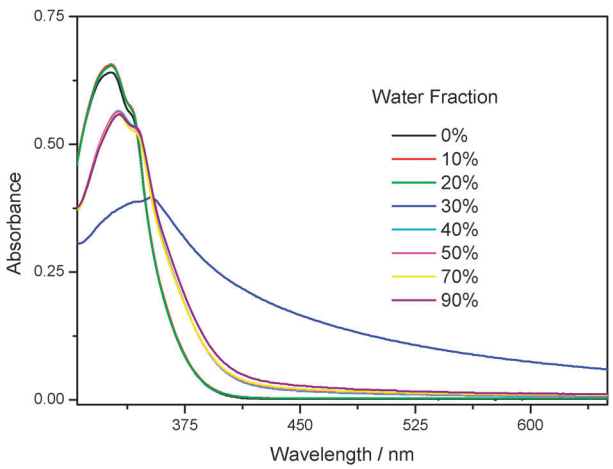

Fig. 2 UV absorption spectra of **2PCz-TPE** in water/DMF mixtures with different volume fractions of water.

fractions, respectively. It will be discussed below that the compound emits blue and green lights in its crystalline and amorphous states, respectively. This phenomenon has been observed in some AIE systems but the reason is not very clear yet.[9] One possible explanation for this phenomenon put forward by Tang's group[10] is that in the mixture with "low" water fraction, the solute molecules steadily assemble in an ordered fashion to form more emissive, bluer crystalline aggregates, and in the mixture with the "high" water content the solute molecules quickly agglomerate in a random way to form less emissive, redder amorphous particles. In the 40–90% water fraction region, there was no obvious change in the PL intensities, suggesting that within the particular region, the aggregates possess the same morphology which was also reflected in their UV spectra and the following fluorescence decay parameters.

Time-resolved emission decay behaviors of the compound in water/DMF mixtures were studied. When the water fraction

Table 1 Fluorescence decay parameters of **2PCz-TPE** in DMF/H_2O with different volume fractions of water

H_2O fraction	$\tau_1{}^a$/ns	$A_1{}^b$	$\tau_2{}^a$/ns	$A_2{}^b$	$\tau_3{}^a$/ns	$A_3{}^b$	$\langle\tau\rangle^c$/ns
30%	0.02	0.25	1.32	0.42	7.89	0.33	3.16
40%	0.89	0.43	2.47	0.57			1.79
50%	0.96	0.45	2.60	0.55			1.86
70%	0.89	0.41	2.54	0.59			1.86
90%	0.93	0.41	2.59	0.59			1.91

[a] Fluorescence lifetime. [b] Fraction contribution. [c] Weighted mean lifetime.

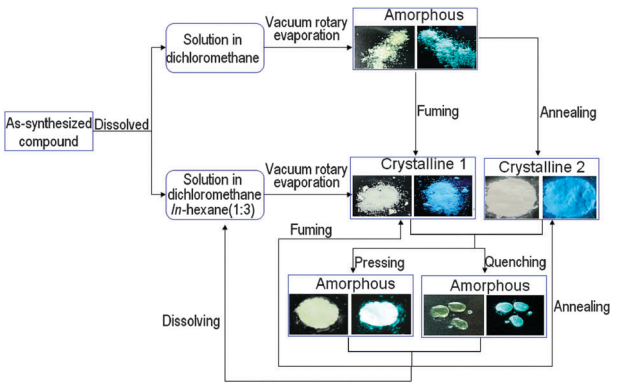

Fig. 3 Schematic representation of the treatment procedures. The pictures in each group were taken at room temperature under ambient light (left) and UV light (right).

was less than 30% (*i.e.* before aggregation), the fluorescence lifetime could not be detected by the equipment. However, when the water fraction was up to 30%, the time-resolved fluorescence curves were obtained and illustrated in Fig. S2 (ESI†), and fluorescence decay parameters are summarized in Table 1. As can be seen from the table, there are two or three relaxation pathways in the fluorescence decays. The mixture with 30% water showed significant difference from the others, which had three relaxation pathways, and its third fluorescence lifetime (τ_3) was up to 7.89 ns. The weighted mean lifetimes $\langle\tau\rangle$ of the mixtures with 40–90% water fraction ranged from 1.79 to 1.91 ns, which showed that the $\langle\tau\rangle$ difference was very little meaning their aggregation structures were the same. However, it was 3.16 ns for the mixture with 30% water fraction. It is suggested that the difference of fluorescence lifetime of the mixtures is caused by the difference of aggregation structures.

To investigate the solid morphology-alterable emission and piezofluorochromic properties, we carried out a series of experiments as schematically illustrated in Fig. 3. Two different aggregates were readily prepared when the solutions of the compound in different solvent systems were evaporated to dryness with a vacuum evaporator. The WAXD result provides convincing evidence and shows that the sample obtained from the solution in dichloromethane/*n*-hexane mixed solvent (1 : 3, v/v) is a crystalline aggregate with some sharp and intense reflections, whereas the sample obtained from dichloromethane solution is an amorphous aggregate with a weak, broad and diffuse peak (Fig. 4).

The DSC heating curve of the amorphous sample shows a cold-crystallization peak at around 136 °C except for a melting

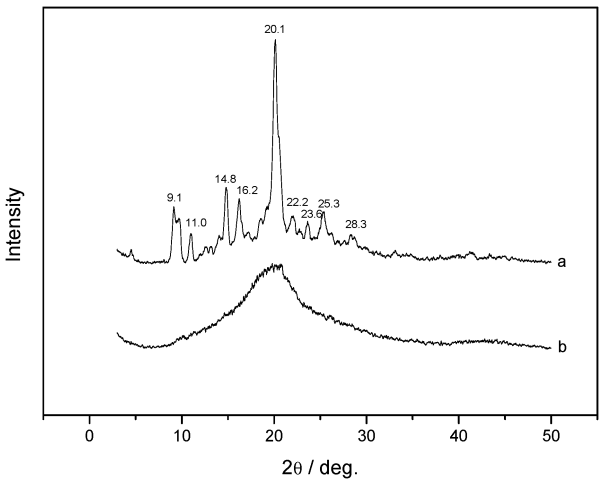

Fig. 4 WAXD curves of the **2PCz-TPE** samples obtained from: (a) dichloromethane/*n*-hexane (1 : 3); (b) dichloromethane.

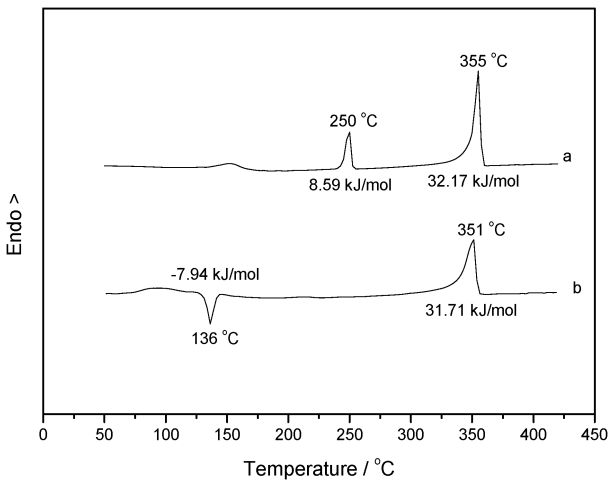

Fig. 5 Heating DSC curves of the **2PCz-TPE** samples obtained from: (a) dichloromethane/*n*-hexane (1 : 3); (b) dichloromethane.

peak at around 351 °C (Fig. 5b). Their transition enthalpies (ΔH) are −7.94 kJ mol^{-1} and 31.71 kJ mol^{-1}, respectively, which means that the crystal corresponding to the melting peak is about 1/4 generated through the cold crystallization. However, the crystalline sample shows two sharp endothermic peaks at 250 °C (ΔH = 8.59 kJ mol^{-1}) and 355 °C (ΔH = 32.17 kJ mol^{-1}); and there is no cold-crystallization peak (Fig. 5a). The ΔH of the two samples in high temperature melting transition are very close. Under a polarized light microscopy with hot-stage, it was observed that the compound is a liquid crystal (Fig. S3, ESI†). The two endothermic peaks around 250 °C and 350 °C correspond to the transitions from solid state to liquid crystalline state and from liquid crystalline state to isotropic melt, respectively.

The crystalline sample is a white powder and the amorphous sample is a light green powder. The crystalline and amorphous samples emit strong blue and green lights, respectively (Fig. 3). As shown in Fig. 6, the maximum emission wavelengths of the crystalline and amorphous samples are 451 nm and 479 nm, respectively. The PL spectrum of amorphous sample exhibits a significant 28 nm red-shift compared with the crystalline

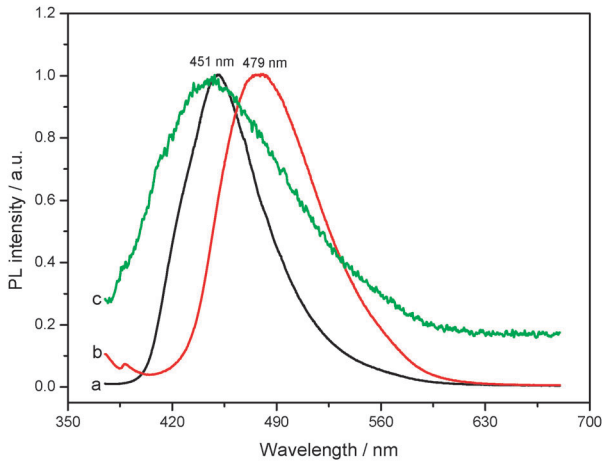

Fig. 6 PL spectra of **2PCz-TPE**: (a) solid sample obtained from dichloromethane/*n*-hexane (1 : 3); (b) solid sample obtained from dichloromethane; (c) dichloromethane solution.

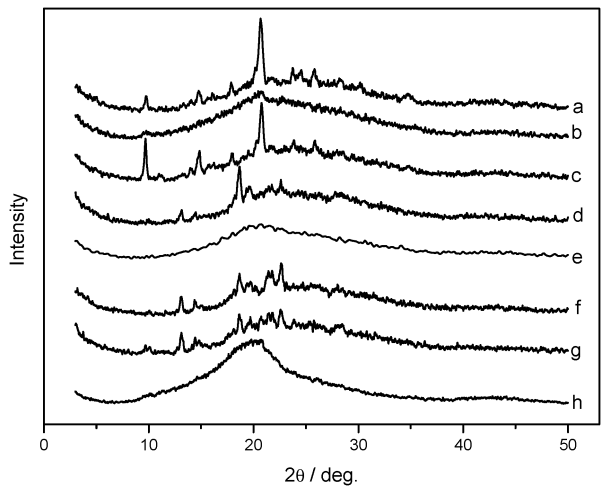

Fig. 7 WAXD patterns of the **2PCz-TPE** samples: (a) obtained from dichloromethane/*n*-hexane (1 : 3); (b) crystalline sample was pressed at 1500 psi; (c) pressed sample was fumed with dichloromethane for 12 h; (d) pressed sample was annealed at 260 °C for 5 min; (e) melt quenched to room temperature; (f) quenched sample was fumed with dichloromethane for 12 h; (g) quenched sample was annealed at 260 °C for 5 min; and (h) obtained from dichloromethane.

sample, which suggests that the molecules in amorphous state have a larger conjugation system than that in crystalline state. The maximum emission wavelength of the crystalline sample is very close to that of dichloromethane solution.

The amorphous sample is changed to the crystalline one when annealed at 260 °C for 5 min or fumed with dichloromethane for about 12 h.

When the crystalline samples were briefly pressed in an IR pellet press by 1500 psi for 1 min, ground using a mortar and pestle, or heated to their melt states and then quenched by liquid nitrogen, they were all changed to the amorphous ones, as confirmed by WAXD with only a diffuse peak (Fig. 7b and e). The PL spectra of the samples obtained by pressing and quenching red-shifted from 451 nm to 479 nm and 493 nm, respectively (Fig. 8). The quenched sample exhibited longer PL wavelength

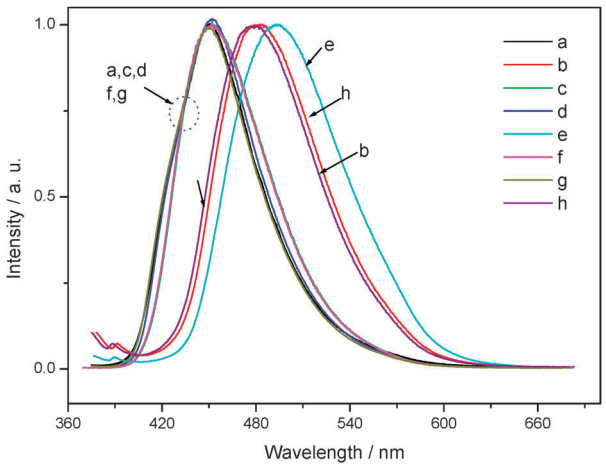

Fig. 8 PL spectra of the **2PCz-TPE** samples: (a) obtained from dichloromethane/*n*-hexane (1 : 3); (b) crystalline sample was pressed at 1500 psi; (c) pressed sample was fumed with dichloromethane for 12 h; (d) pressed sample was annealed at 260 °C for 5 min; (e) melt quenched to room temperature; (f) quenched sample was fumed with dichloromethane for 12 h; (g) quenched sample was annealed at 260 °C for 5 min; and (h) obtained from dichloromethane.

than the pressed sample. The result obtained from the pressing treatment indicates that the compound has a significant piezofluorochromic property. The possible mechanism will be discussed in the single crystal X-ray diffraction analysis section.

The DSC results show that heating DSC curves of the pressed and quenched samples (Fig. 9b and e) are considerably different from the original crystalline sample (Fig. 9a). Similar to the amorphous sample (Fig. 9h), the pressed and quenched samples also show cold-crystallization peaks at 118 °C and 242 °C, respectively, followed by the melting peak at around 354 °C. The new cold-crystallization peaks might be ascribed to a phase-to-phase transition, which suggests that the pressing

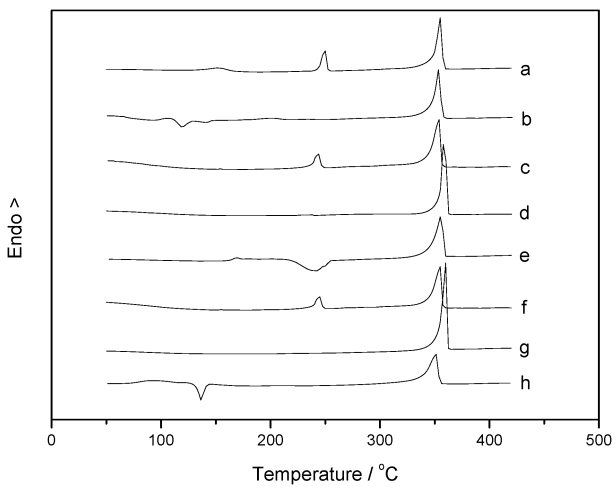

Fig. 9 DSC heating curves of the **2PCz-TPE** samples: (a) obtained from dichloromethane/*n*-hexane (1 : 3); (b) crystalline sample was pressed at 1500 psi; (c) pressed sample was fumed with dichloromethane for 12 h; (d) pressed sample was annealed at 260 °C for 5 min; (e) melt quenched to room temperature; (f) quenched sample was fumed with dichloromethane for 12 h; (g) quenched sample was annealed at 260 °C for 5 min; and (h) obtained from dichloromethane.

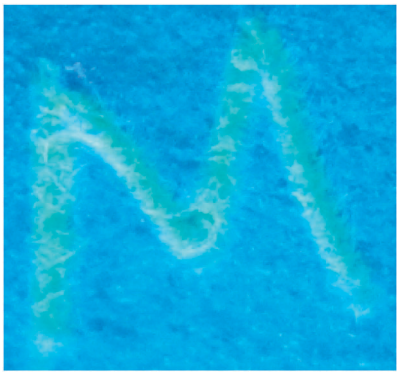

Fig. 10 The image taken at room temperature under 365 nm UV light: **2PCz-TPE** is cast on a filter paper and written "M" with a metal spatula.

and quenching treatments can convert the thermodynamically stable phase to metastable states. The melting peak temperatures of the latter two are almost the same. However, the quenched sample exhibits 124 °C higher cold-crystallization temperature than the pressed sample, which might reflect the variability in some degree of the two metastable states.

The amorphous samples obtained by pressing and quenching treatments can be reverted to the crystalline ones by fuming with dichloromethane for less than 12 h. The WAXD results show that the original sample (Fig. 7a) and the fumed samples (Fig. 7c and f) are the same, and the DSC experiments (Fig. 9a, c and f) also show the same results, indicating that the compound exhibits good morphological reversibility between crystalline state and amorphous state. The reversible behavior can be completely achieved through solvent vapor-induced crystallization and pressure-destroyed crystalline structure. Although the morphological change from amorphous state to crystalline state can be realized by annealing, the crystalline structure is slightly different from the original and fumed samples. This result is profoundly manifested in the corresponding WAXD and DSC curves. The original and fumed samples show a sharp diffraction peak at around $2\theta = 9°$ in their WAXD curves and an endothermic peak at ~243 °C in their DSC curves. The annealed samples have no such peaks,

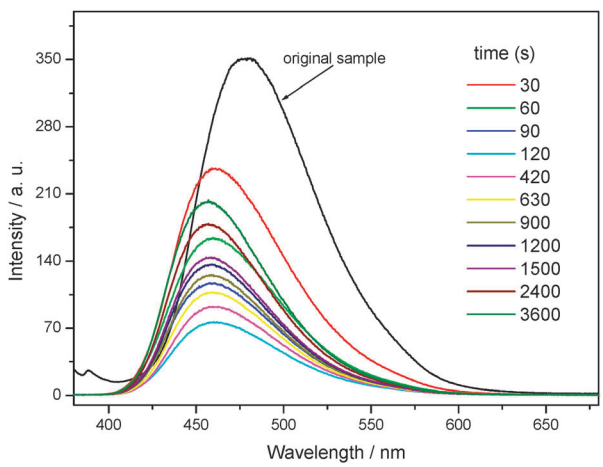

Fig. 11 PL spectra of the amorphous sample under fuming with dichloromethane vapor. (Note: except the original sample curve, the others were detected online.)

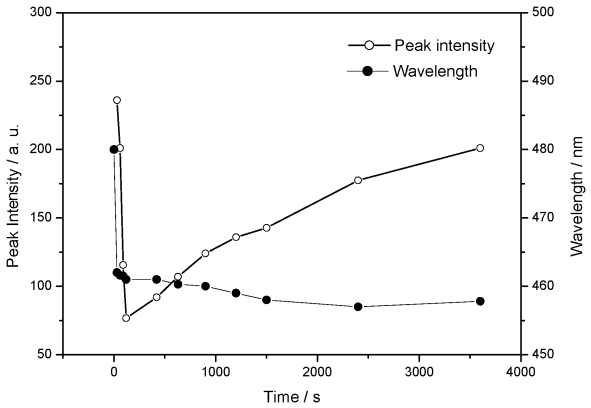

Fig. 12 PL peak intensity and wavelength *vs.* fuming time with dichloromethane.

suggesting that the completely reversible cycle cannot be achieved by the annealing treatment. Except for by a fuming treatment method, the reversible behavior also can be achieved by dissolving the amorphous samples in dichloromethane/*n*-hexane mixed solvent (1 : 3, v/v) and then evaporating the solution to dryness with a vacuum evaporator.

The solution of **2PCz-TPE** in dichloromethane/*n*-hexane (1 : 3) was cast on a filter paper. After drying, we wrote "M" with a metal spatula on the paper (Fig. 10). A green "M" stamp on the blue "paper" under the UV lamp (365 nm) can be seen. The result suggests that the material has a potential application as an optical recording material.[11]

Fig. 11 and 12 show the relationship of the PL peak intensity and wavelength with dichloromethane fuming time. The PL peak intensity of the amorphous sample decreased rapidly from 30 s to 120 s. After 120 s, the intensity gradually increased with prolonged fuming time. At first, the permeation of the good solvent during fuming can weaken the interaction of **2PCz-TPE** molecules due to solvation, leading to the

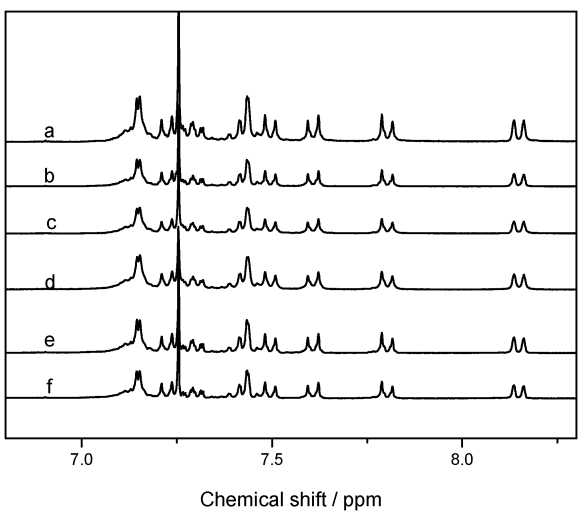

Fig. 13 ^{1}H NMR of **2PCz-TPE** samples (in $CDCl_3$) (a) obtained from dichloromethane; (b) obtained from dichloromethane/*n*-hexane (1 : 3); (c) crystalline sample was pressed at 1500 psi for 1 min; (d) pressed sample was fumed with dichloromethane for 12 h; (e) pressed sample was annealed at 260 °C for 5 min; (f) melt quenched to room temperature.

increase in intramolecular rotational and vibrational motions, the increase in non-emissive decay of excited state energy, and, consequently, the decrease in the PL intensity. Almost at the same time, solvent-induced crystallization took place. As the degree of crystallization progressed, the molecules became more compact, leading to the restriction of the intramolecular vibrations and rotations, the occurrence of crystallization-induced emission enhancement effect, and, consequently, the increase in PL intensity. Thus, the two opposite effects made the curve V-shape, depending on which effect played a dominant role in the whole PL behavior. The PL behavior was quite different from the triphenylamine–tetraphenylethylene compound (TPA–TPE) whose PL intensity decreased and PL wavelength red-shifted with dichloromethane fuming time.[7c]

The wavelength exhibited abrupt blue-shifts from 479 to 462 nm within 30 s (the change was very fast, and shorter time could not be obtained because the operation and scanning procedure of PL needed time) indicating that the sample was very sensitive to the solvent vapor and had potential applications as an organic vapor sensor; afterwards, it became flat. We considered that the abrupt blue-shifts were caused by solvent induced crystallization.

To verify whether the chemical structure of **2PCz-TPE** changed after heating, fuming and pressing, ^{1}H-NMR experiments in $CDCl_3$ were conducted. Fig. 13 shows that the ^{1}H-NMR spectra were almost the same, indicating that the chemical structure did not change. This further suggests that the different spectroscopic properties and morphological structures of **2PCz-TPE** are caused by physical processes (*i.e.*, by changing the mode of molecular packing).

The single crystals of **2PCz-TPE** were successfully grown from the solutions of dichloromethane/*n*-hexane mixture and their crystal structure was determined by single-crystal X-ray diffraction analysis. The selected crystallographic data are given in Table 2. After checking the single-crystal X-ray diffraction analysis results, it is found that there are many cavities in the single crystal and the cavities are filled with solvent molecules. The solvent molecules are highly disordered. The asymmetric unit includes 0.5 half hexane molecules with an inversion center located at the center of the hexane molecule, 0.25 CH_2Cl_2 molecules and 0.4 water molecules, together with one molecule of **2PCz-TPE**.

Table 2 Crystal data and structure refinement for the single crystal

Identification	
Formula	$C_{127.5}H_{84}N_4O_{0.8}Cl$
F.w.	1720.24
T/K	110(2)
Crystal system, space group	Triclinic, $P\bar{1}$
a/Å	11.0164(17)
b/Å	11.8961(18)
c/Å	18.841(3)
α/°	81.814(3)
β/°	84.930(3)
γ/°	69.902(3)
V/Å^3	2293.1(6)
Z	1
$d_{calc.}$/g cm^{-3}	1.246
μ/mm^{-1}	0.100
F(000)	900
Crystal size/mm^3	0.44 × 0.40 × 0.25
θ Range for data collection	1.09–27.09
Index range	$-14 \le h \le 14$, $-15 \le k \le 15$, $-24 \le l \le 23$
Data collected/uniq. (R_{int})	19 213/9791 (0.0320)
Data/restraints/parameters	9791/50/639
R_1 (wR_2)^a, [$I > 2\theta(I)$]	0.0580 (0.1601)
R_1 (wR_2)^a, (all data)	0.1071 (0.1972)
GOF on F^2	1.033
Largest diff. peak and hole/e·Å^{-3}	0.602–0.371

^{a} $R_1 = \Sigma||F_o|-|F_c||/\Sigma|F_o|$. w$R_2 = [\Sigma[w(F_o^2 - F_c^2)^2]/\Sigma w(F_o^2)^2]^{1/2}$.

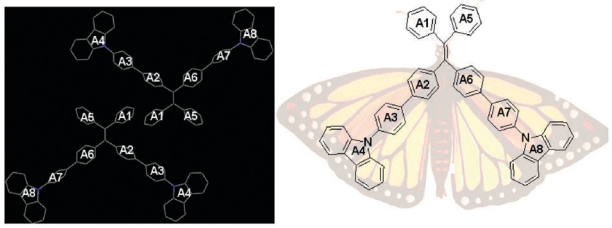

Fig. 14 The crystal structure of the compound with defined planes (left), and the "butterfly-shaped" molecule (right).

Table 3 The dihedral angles of the selected planes of the molecule in the single crystal and free molecule

	Dihedral angle/°			Dihedral angle/°	
Plane	Single crystal^a	Free molecule^b	Plane	Single crystal^a	Free molecule^b
A_1–A_2	54	57	A_5–A_6	56	57
A_1–A_5	85	75	A_2–A_6	85	75
A_1–A_6	82	77	A_2–A_5	62	77
A_2–A_3	20	36	A_6–A_7	27	36
A_3–A_4	45	56	A_7–A_8	74	56

^{a} Geometry from the single crystal. ^{b} Geometry from calculation using GAUSSIAN 03.

Geometry of the isolated free molecule of the compound in the ground state was optimized based on B3LYP/6-31G calculation using GAUSSIAN 03 package program.[12] Based on the optimized

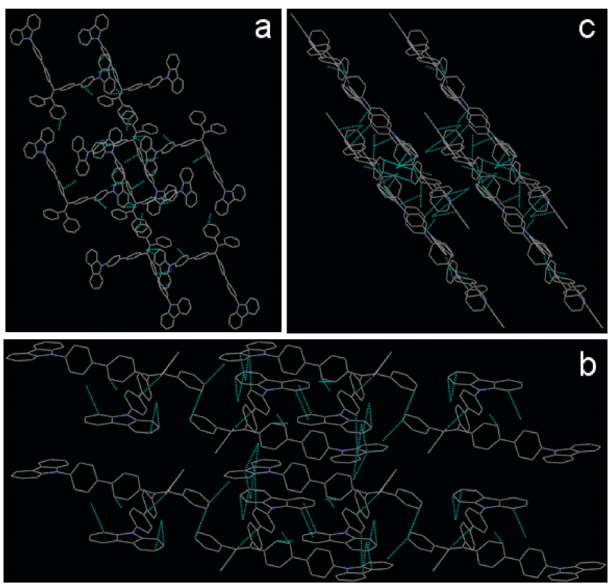

Fig. 15 Crystal packing viewed along *a*-axis (a), *b*-axis (b) and *c*-axis (c) for **2PCz-TPE** (the hydrogen atoms, and the solvent molecules located between the layers have been omitted for clarity; the green dotted lines represent π–π and C–H–π interactions).

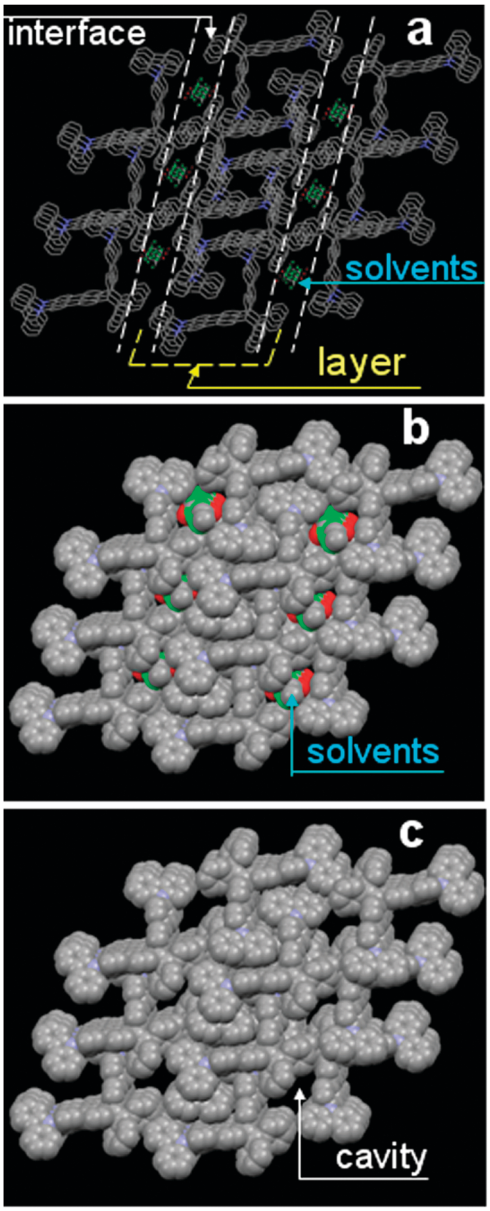

Fig. 16 Molecules packing in the single crystal: (a) capped sticks style and (b) spacefill style showing inclusion of dichloromethane/*n*-hexane between the layers; (c) spacefill style with solvent molecules removed (the hydrogen atoms have been omitted for clarity).

geometry, the dihedral angles between the aryl rings as defined in Fig. 14 were calculated and collected in Table 3. Although the isolated free molecule has a twisted conformation, the dihedral angles of each phenyl ring pair, A_1–A_2 (A_5–A_6), A_1–A_5 (A_2–A_6), A_1–A_6 (A_2–A_5), A_2–A_3 (A_6–A_7) and A_3–A_4 (A_7–A_8), are the same. For example, A_2–A_3 and A_6–A_7 have the same dihedral angle of 36°. In comparison, the crystalline structure shows the "butterfly-shaped" molecules (see Fig. 14) that are packed in a head-to-head fashion. Due to the highly twisted conformation of tetraphenylethylene and steric hindrance of the bulky carbazole rings in the molecule, the interaction of each aromatic ring (or plane) is different. For example, in the crystalline structure, it can be seen clearly that face-to-face π–π interaction exists between the A_1 phenyl rings of two packing molecules and there are no π–π interaction between two A_5 phenyl rings, although the A_1 phenyl ring and the A_5 phenyl ring are the same chemically. Thus, the dihedral angles for the phenyl ring pairs are different and some of them show a remarkable difference. For example, the dihedral angles of A_3–A_4 and A_7–A_8 pairs are 45° and 74°, respectively. The difference is up to 29°. The difference between single-crystal structure and isolated molecule indicates that the molecules in the single crystal exhibit a more highly twisted conformation than in the isolated state.

As mentioned above, due to the highly twisted conformation, the backbone of the molecule largely deviates from a plane and typical cofacial π–π stacking becomes impossible. However, as depicted in Fig. 15, the molecules are packed *via* synergetic weak π–π and C–H–π interactions (wing part of the "butterfly-shaped" molecule), which form lamellar layer structures. The layers are subsequently connected *via* antenna parts of the "butterfly-shaped" molecules with weaker π–π interactions (only A_1-ring interactions). Due to the twisted conformation and weaker π–π interactions, the interfaces between the layers are relatively loose and there exist some defects (cavities).

As shown in Fig. 16, each unit cell contains solvent molecules which are filled in the cavity of interface (Fig. 16a, capped sticks style; Fig. 16b, spacefill style). Each cavity located between the layers is suitable for accommodating solvent molecules. Due to weaker interactions and the cavities existing in the interfaces, the interfaces are the feeblest parts in the crystalline structures. Thus, the interfaces are readily destroyed by external pressure, which may be triggered by slip deformation under external pressure. The crash of crystalline structure leads to the release of crystal lattice energy which is an important binding force to maintain the highly twisted molecular conformation in the crystalline state. The decrease or disappearance of the crystal lattice binding force can therefore cause the planarization of molecular conformation, which is evidenced by the increase of molecular conjugation thus resulting in a red-shift of PL spectrum. These, in terms of a molecular mechanism, may explain the piezofluorochromic behavior of this PAIE compound.

Conclusions

A new piezofluorochromic aggregation-induced emission compound containing tetraphenylethylene and carbazole moieties was synthesized. The spectroscopic properties and morphological structures of the compound were reversed upon pressing or fuming. The PL spectra of the samples obtained by annealing and by fuming were different. The results show that the piezofluorochromic nature is generated from crystalline–amorphous phase transformation under external pressure. The reason for the phase transformation is ascribed to poor solid molecular packing and formation of some cavities in the interfaces of lamellar layers which was confirmed by the single crystal X-ray diffraction analysis.

Acknowledgements

The authors gratefully acknowledge the financial support from the National Natural Science Foundation of China (51173210, 51073177), the Start-up Fund for Recruiting Professionals

from "985 Project" of SYSU, the Science and Technology Planning Project of Guangdong Province, China (Grant numbers: 2007A010500001-2, 2008B090500196), Construction Project for University-Industry cooperation platform for Flat Panel Display from The Commission of Economy and Informatization of Guangdong Province (Grant number: 20081203), the Fundamental Research Funds for the Central Universities and Natural Science Foundation of Guangdong (S2011020001190).

Notes and references

1 (*a*) Y. Sagara, T. Mutai, I. Yoshikawa and K. Araki, *J. Am. Chem. Soc*., 2007, **129**, 1520; (*b*) T. Mutai, H. Satou and K. Araki, *Nat. Mater*., 2005, **4**, 685; (*c*) J. Kunzelman, M. Kinami, B. R. Crenshaw, J. D. Protasiewicz and C. Weder, *Adv. Mater*., 2008, **20**, 119; (*d*) Y. Muramatsu, T. Yamamoto, M. Hasegawa, T. Yagi and H. Koinuma, *Polymer*, 2001, **42**, 6673; (*e*) R. Gawinecki, R. Dobosz and A. Zakrewska, *Dyes Pigm*., 2004, **60**, 143; (*f*) S. Mizukami, H. Hojou, K. Sugaya, E. Koyama, H. Tokuhisa, T. Sasaki and M. Kanesato, *Chem. Mater*., 2005, **17**, 50.

2 (*a*) H. Y. Li, X. Q. Zhang, Z. G. Chi, B. J. Xu, W. Zhou, S. W. Liu, Y. Zhang and J. R. Xu, *Org. Lett*., 2011, **13**, 556; (*b*) X. Q. Zhang, Z. G. Chi, H. Y. Li, B. J. Xu, X. F. Li, W. Zhou, S. W. Liu, Y. Zhang and J. R. Xu, *Chem.–Asian J*., 2011, **6**, 808; (*c*) H. Y. Li, Z. G. Chi, B. J. Xu, X. Q. Zhang, X. F. Li, S. W. Liu, Y. Zhang and J. R. Xu, *J. Mater. Chem*., 2011, **21**, 3760; (*d*) X. Q. Zhang, Z. G. Chi, J. Y. Zhang, H. Y. Li, B. J. Xu, X. F. Li, S. W. Liu, Y. Zhang and J. R. Xu, *J. Phys. Chem. B*, 2011, **115**, 7606.

3 J. Luo, Z. Xie, J. W. Y. Lam, L. Cheng, H. Chen, C. Qiu, H. S. Kwok, X. Zhan, Y. Liu, D. Zhu and B. Z. Tang, *Chem. Commun*., 2001, 1740.

4 (*a*) Y. N. Hong, J. W. Y. Lam and B. Z. Tang, *Chem. Commun*., 2009, 4332; (*b*) Y. S. Zhao, H. Fu, A. Peng, Y. Ma, D. Xiao and J. Yao, *Adv. Mater*., 2008, **20**, 2859; (*c*) X. Q. Zhang, Z. Y. Yang, Z. G. Chi, M. N. Chen, B. J. Xu, C. C. Wang, S. W. Liu, Y. Zhang and J. R. Xu, *J. Mater. Chem*., 2010, **20**, 292.

5 (*a*) Z. Y. Yang, Z. G. Chi, T. Yu, X. Q. Zhang, M. N. Chen, B. J. Xu, S. W. Liu, Y. Zhang and J. R. Xu, *J. Mater. Chem*., 2009, **19**, 5541; (*b*) B. K. An, D. S. Lee, J. S. Lee, Y. S. Park, H. S. Song and S. Y. Park, *J. Am. Chem. Soc*., 2004, **126**, 10232; (*c*) J. W. Chen, B. Xu, X. Y. Ouyang, B. Z. Tang and Y. Cao, *J. Phys. Chem. A*, 2004, **108**, 7522; (*d*) J. W. Chen, C. C. W. Law, J. W. Y. Lam, Y. P. Dong, S. M. F. Lo, I. D. Williams, D. B. Zhu and B. Z. Tang, *Chem. Mater*., 2003, **15**, 1535; (*e*) Y. Ren, J. W. Y. Lam, Y. Dong, B. Z. Tang and K. S. Wong, *J. Phys. Chem. B*, 2005, **109**, 1135; (*f*) H. Y. Li, Z. G. Chi, B. J. Xu, X. Q. Zhang, Z. Y. Yang, X. F. Li, S. W. Liu, Y. Zhang and J. R. Xu, *J. Mater. Chem*., 2010, **20**, 6103; (*g*) F. Wang, M. Y. Han, K. Y. Mya, Y. Wang and Y. H. Lai, *J. Am. Chem. Soc*., 2005, **127**, 10350; (*h*) K. Itami, Y. Ohashi and J. I. Yoshida, *J. Org. Chem*., 2005, **70**, 2778; (*i*) C. J. Bhongale, C. W. Chang, C. S. Lee, E. W. G. Diau and C. S. Hsu, *J. Phys. Chem. B*, 2005, **109**, 13472; (*j*) J. T. He, B. Xu, F. P. Chen, H. J. Xia, K. P. Li, L. Ye and W. J. Tian, *J. Phys. Chem. C*, 2009, **113**, 9892; (*k*) X. Q. Zhang, Z. G. Chi, H. Y. Li, B. J. Xu, X. F. Li, S. W. Liu, Y. Zhang and J. R. Xu, *J. Mater. Chem*., 2011, **21**, 1788; (*l*) X. Q. Zhang, Z. G. Chi, B. J. Xu, H. Y. Li, Z. Y. Yang, X. F. Li, S. W. Liu, Y. Zhang and J. R. Xu, *Dyes Pigm*., 2011, **89**, 56; (*m*) X. Q. Zhang, Z. G. Chi, B. J. Xu, H. Y. Li, W. Zhou, X. F. Li, Y. Zhang, S. W. Liu and J. R. Xu, *J. Fluoresc*., 2011, **21**, 133; (*n*) B. J. Xu, Z. G. Chi, X. F. Li, H. Y. Li, X. Q. Zhang, W. Zhou, C. C. Wang, Y. Zhang, S. W. Liu and J. R. Xu, *J. Fluoresc*., 2011, **21**, 433; (*o*) Z. Y. Yang, Z. G. Chi, B. J. Xu, H. Y. Li, X. Q. Zhang, X. F. Li, S. W. Liu, Y. Zhang and J. R. Xu, *J. Mater. Chem*., 2010, **20**, 7352; (*p*) X. Q. Zhang, Z. Y. Yang, Z. G. Chi, M. N. Chen, B. J. Xu, C. C. Wang, S. W. Liu, Y. Zhang and J. R. Xu, *J. Mater. Chem*., 2010, **20**, 292; (*q*) B. J. Xu, Z. G. Chi, Z. Y. Yang, J. B. Chen, S. Z. Deng, H. Y. Li, X. F. Li, Y. Zhang, N. S. Xu and J. R. Xu, *J. Mater. Chem*., 2010, **20**, 4135; (*r*) H. Y. Li, Z. G. Chi, X. Q. Zhang, B. J. Xu, S. W. Liu, Y. Zhang and J. R. Xu, *Chem. Commun*., 2011, **47**, 11273; (*s*) B. J. Xu, Z. G. Chi, H. Y. Li, X. Q. Zhang, X. F. Li, S. W. Liu, Y. Zhang and J. R. Xu, *J. Phys. Chem. C*, 2011, **115**, 17574; (*t*) X. F. Li, Z. G. Chi, B. J. Xu, H. Y. Li, X. Q. Zhang, W. Zhou, Y. Zhang, S. W. Liu and J.R. Xu, *J. Fluoresc*., 2011, **21**, 1969.

6 (*a*) S. J. Yoon, J. W. Chung, J. Gierschner, K. S. Kim, M. G. Choi, D. Kim and S. Y. Park, *J. Am. Chem. Soc*., 2010, **132**, 13675; (*b*) C. D. Dou, L. Han, S. S. Zhao, H. Y. Zhang and Y. Wang, *J. Phys. Chem. Lett*., 2011, **2**, 666; (*c*) C. D. Dou, D. Chen, J. Lqbal, Y. Yuan, H. Y. Zhang and Y. Wang, *Langmuir*, 2011, **27**, 6323.

7 (*a*) Z. J. Zhao, S. M. Chen, X. Y. Shen, F. Mahtab, Y. Yu, P. Lu, J. W. Y. Lam, H. S. Kwok and B. Z. Tang, *Chem. Commun*., 2010, **46**, 686; (*b*) B. J. Xu, Z. G. Chi, J. Y. Zhang, X. Q. Zhang, H. Y. Li, X. F. Li, S. W. Liu, Y. Zhang and J. R. Xu, *Chem.–Asian J*., 2011, **6**, 1470; (*c*) X. Zhou, H. Y. Li, Z. G. Chi, B. J. Xu, X. Q. Zhang, Y. Zhang, S. W. Liu and J. R. Xu, *J. Fluoresc*., 2011, DOI: 10.1007/s10895-011-0990-4.

8 G. M. Sheldrick, *SHELX-97, Program for crystal structure solution and refinement*, University of Götingen, Götingen, Germany, 1997.

9 (*a*) Y. Q. Dong, J. W. Y. Lam, A. J. Qin, Z. Li, J. Z. Sun, H. H. Y. Sung, I. D. Williams and B. Z. Tang, *Chem. Commun*., 2007, 40; (*b*) Y. Q. Dong, J. W. Y. Lam, A. J. Qin, J. X. Sun, J. Z. Liu, Z. Li, J. Z. Sun, H. H. Y. Sung, I. D. Williams, H. S. Kwok and B. Z. Tang, *Chem. Commun*., 2007, 3255; (*c*) H. Tong, Y. N. Hong, Y. Q. Dong, Y. Ren, M. Häußler, J. W. Y. Lam, K. S. Wong and B. Z. Tang, *J. Phys. Chem. B*, 2007, **111**, 2000; (*d*) H. Tong, Y. Q. Dong, M. Häußler, J. W. Y. Lam, H. H. Y. Sung, I. D. Williams, J. Z. Sun and B. Z. Tang, *Chem. Commun*., 2006, 1133; (*e*) J. Z. Liu, J. W. Y. Lam and B. Z. Tang, *J. Inorg. Organomet. Polym*., 2009, **19**, 249.

10 Y. Q. Dong, J. W. Y. Lam, A. J. Qin, J. X. Sun, J. Z. Liu, Z. Li, J. Z. Sun, H. H. Y. Sung, I. D. Williams, H. S. Kwok and B. Z. Tang, *Chem. Commun*., 2007, 3255.

11 (*a*) H. Ito, T. Saito, N. Oshima, N. Kitamura, S. Ishizaka, Y. Hinatsu, M. Wakeshima, M. Kato, K. Tsuge and M. Sawamura, *J. Am. Chem. Soc*., 2008, **130**, 10044; (*b*) Y. Sagara, S. Yamane, T. Mutai, K. Araki and T. Kato, *Adv. Funct. Mater*., 2009, **19**, 1869; (*c*) Y. Zhao, H. Gao, Y. Fan, T. Zhou, Z. Su, Y. Liu and Y. Wang, *Adv. Mater*., 2009, **21**, 3165; (*d*) N. S. S. Kumar, S. Varghese, N. P. Rath and S. Das, *J. Phys. Chem. C*, 2008, **112**, 8429; (*e*) Y. Sagara and T. Kato, *Angew. Chem., Int. Ed*., 2008, **47**, 5175; (*f*) T. Tsukuda, M. Kawase, A. Dairiki, K. Matsumoto and T. Tsubomura, *Chem. Commun*., 2010, **46**, 3255; (*g*) G. Zhang, J. Lu, M. Sabat and C. L. Fraser, *J. Am. Chem. Soc*., 2010, **132**, 2160; (*h*) Y. Ooyama, G. Ito, H. Fukuoka, T. Nagano, Y. Kagawa, I. Imae, K. Komaguchi and Y. Harima, *Tetrahedron*, 2010, **66**, 7268; (*i*) S. Perruchas, X. F. Le Goff, S. Maron, I. Maurin, F. Guillen, A. Garcia, T. Gacoin and J. P. Boilot, *J. Am. Chem. Soc*., 2010, **132**, 10967; (*j*) Y. Ooyama, Y. Kagawa, H. Fukuoka, G. Ito and Y. Harima, *Eur. J. Org. Chem*., 2009, 5321.

12 M. J. Frisch, G. W. Trucks and H. B. Schlegel, *et al*., *Gaussian 03. Revision D.01*, Gaussian, Inc., Wallingford, CT, 2004.